Journal of Medicinal Chemistry

ARTICLE

pubs.acs.org/jmc

Synthesis and Evaluation of Novel Carbon-11 Labeled Oxopurine Analogues for Positron Emission Tomography Imaging of Translocator Protein (18 kDa) in Peripheral Organs

Katsushi Kumata,[†] Joji Yui,[†] Akiko Hatori,[†] Masayuki Fujinaga,[†] Kazuhiko Yanamoto,[†] Tomoteru Yamasaki,[†] Kazunori Kawamura,[†] Hidekatsu Wakizaka,[†] Nobuki Nengaki,[†,‡] Yuichiro Yoshida,[†,‡] Masanao Ogawa,[†,‡] Toshimitsu Fukumura,[†] and Ming-Rong Zhang*[,†]

[†]Department of Molecular Probes, Molecular Imaging Center, National Institute of Radiological Sciences, 4-9-1 Anagawa, Inage-ku, Chiba 263-8555, Japan

[‡]SHI Accelerator Service Co. Ltd., 5-9-11 Kitashinagawa, Shinagawa-ku, Tokyo 141-8686, Japan

Supporting Information

ABSTRACT: To develop a PET ligand for imaging TSPO in peripheral organs, we designed three novel oxopurine analogues [^{11}C]**3a**−**c** (LogD: 1.81−2.17) by introducing a pyridine ring in place of a benzene ring in the lead compound [^{11}C]**2** (LogD: 3.48). The desmethyl precursors **10** for radiosynthesis were synthesized by reacting glycine **7** with picolylamines **4**, followed by hydrolysis and by Curtius rearrangement with diphenylphosphoryl azide. Methylation of **10a**−**c** with methyl iodide produced unlabeled compounds **3a**−**c**. The radiosynthesis of [^{11}C]**3a**−**c** was performed by reacting **10a**−**c** with [^{11}C]methyl iodide. Compounds **3a**−**c** displayed high or moderate in vitro binding affinities (K_i: 5−40 nM) for TSPO. PET with [^{11}C]**3a**−**c** in rats showed high uptake in the lung, heart, and kidney, which are organs with high TSPO expression. Metabolite analysis with [^{11}C]**3a** showed that radioactivity in these organs mainly corresponded with unchanged [^{11}C]**3a**. PET with [^{11}C]**3a** using a rat model of lung inflammation showed a significant signal in the lipopolysaccharide-treated lung.

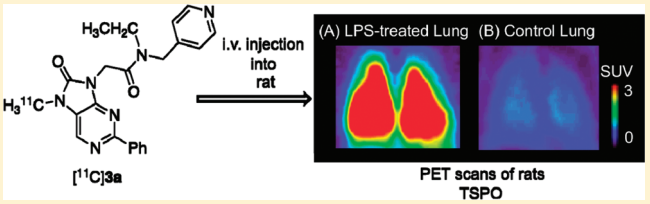

INTRODUCTION

Translocator protein (18 kDa) (TSPO, formerly known as the peripheral-type benzodiazepine receptor, PBR) is located on the mitochondrial outer membrane in several organs, including the lung, heart, kidney, and endocrine organs such as the adrenal, testis, and pituitary gland.[1] A low level of TSPO was also found in microglia cells of the brain.[1−3] It has been demonstrated that TSPO has wide functions related to the regulation of cholesterol transport and synthesis of steroid hormones, porphyrin transport and heme synthesis, apoptosis, cell proliferation, anion transport, regulation of mitochondrial functions, immunomodulation, and inflammation.[1,3]

Visualization of the immune response with molecular imaging probes specific to immune cells could enhance understanding of the cellular mechanism of various inflammatory diseases. Imaging probes using various modalities have been developed to visualize and detect autoimmune disease, neuroinflammation, inflammatory arthritides, cardiovascular system, and cancer.[4−7] Among these imaging probes, positron emission tomography (PET) ligands for TSPO are becoming potential and specific tools which have been used to visualize inflammation and elucidate the relationalship between TSPO and various inflammatory diseases.[5−9]

(*R*)-(1-(2-Chlorophenyl)-*N*-[^{11}C]methyl,*N*-(1-methylpropyl)-isoquinoline ([^{11}C](*R*)-PK 11195, [^{11}C]**1**, Scheme 1) was the first PET ligand used for imaging TSPO in neuroinflammation.[10] However, [^{11}C]**1** had several limitations, such as relatively low brain uptake, high nonspecific binding, and high lipophilicity.[11] To investigate TSPO precisely using a PET ligand with improvement over [^{11}C]**1**, several dozen ^{11}C and ^{18}F-labeled radioligands have been reported.[12−16] We have developed a new PET ligand, *N*-benzyl-*N*-ethyl-2-(7,8-dihydro-7-[^{11}C]methyl-8-oxo-2-phenyl-9*H*-purin-9-yl)acetamide ([^{11}C]AC-5216, [^{11}C]**2**; Scheme 1), for imaging TSPO in the human brain.[17,18] However, [^{11}C]**2**, like [^{11}C]**1**, had rather slow kinetics in the brain and did not show a decrease of radioactivity in the brain within the PET scan, which limited its usefulness for quantitative analysis of TSPO.[18,19] High lipophilicity (LogD: 3.48) and potent binding affinity (K_i: 0.6 nM for TSPO)[20] of [^{11}C]**2** were considered the partial causes of the shortcomings.

In this study, using [^{11}C]**2** as a lead compound, we designed three novel oxopurine analogues [^{11}C]**3a**−**c** (Scheme 1) and evaluated their potential as PET ligands for imaging TSPO. As shown in the chemical structures, a pyridine ring was introduced into [^{11}C]**3a**−**c** instead of a benzene ring in [^{11}C]**2**. This structural change may decrease lipophilicity of [^{11}C]**3a**−**c**, so these radioligands may be expected to show improved kinetics

Received: April 28, 2011
Published: July 26, 2011

dx.doi.org/10.1021/jm200516a | *J. Med. Chem.* 2011, 54, 6040–6049

and have lower nonspecific binding in the targeted tissues than [^{11}C]**2**.

On the other hand, with the recognition that TSPO plays an important role in regulating immune response,[1,3,4] we used [^{11}C]**3a**−**c** to elucidate in vivo specific binding for TSPO in the peripheral organs and to visualize lung inflammation in the present study. To our knowledge, there were few reports of PET studies with TSPO radioligands for imaging lung inflammation.[21,22] Because TSPO is present in the peripheral organs at high density (B_{max}: 141 pmol/mL in lung, 393 pmol/mL in heart, and 158 pmol/mL in kidney),[23] moderate binding affinity of a PET ligand may be enough to determine in vivo specific binding for TSPO in these organs.

Here, we report: (1) the chemical synthesis of novel unlabeled compounds **3a**−**c**, (2) the radiosynthesis of [^{11}C]**3a**−**c**, (3) the in vitro binding affinity (K_i) with TSPO and lipophilicity, (4) the kinetics and in vivo specific binding for TSPO in the peripheral organs of rats using small-animal PET with [^{11}C]**3a**−**c**, (5) the in vivo metabolite analysis with [^{11}C]**3a** in the plasma, liver, lung, heart, and kidney, and (6) the visualization of lung inflammation using PET with [^{11}C]**3a** in a rat model which was induced by lipopolysaccharide (LPS).

Scheme 1. Chemical Structures of PET Ligands for TSPO

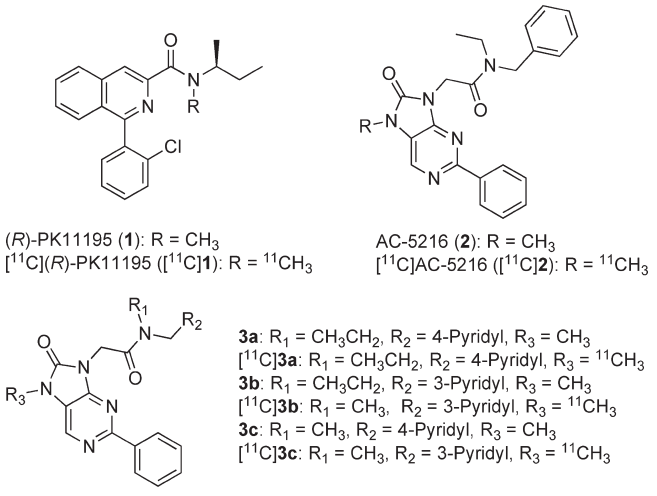

RESULTS AND DISCUSSION

Chemistry. Novel oxopurine analogues **3a**−**c** were synthesized as shown in Scheme 2. Picolylamines **4a**−**c** were synthesized by reducing Schiff's base **6**, which was prepared by condensation of pyridinecarboxaldehyde **5** with methyl- or ethylamine. The glycine compound **7**, which was prepared according to procedures described previously,[24] reacted with **4a**−**c** in the presence of (benzotriazol-1-yloxy)tris(dimethylamino)phosphonium hexafluorophosphate (BOP) to afford amide **8**. Hydrolysis of **8** with NaOH gave carboxylic acid **9**, followed by Curtius rearrangement with diphenylphosphoryl azide to produce **10** in chemical yields of 46−73%. The unlabeled compounds **3a**−**c** were prepared by reacting **10** with methyl iodide (MeI) in *N*,*N*-dimethylforamide (DMF) using K_2CO_3 as a base.

Radiosynthesis of [^{11}C]**3a**−**c** was performed using a home-made automated synthesis system.[25] The labeling agent [^{11}C]methyl iodide ([^{11}C]MeI) was prepared by reducing cyclotron-produced [^{11}C]carbon dioxide ([^{11}C]CO_2) with lithium aluminum hydride ($LiAlH_4$), followed by iodination with 57% hydroiodic acid.[25,26] The produced [^{11}C]MeI was purified by distillation and trapped in a DMF solution of desmethyl precursor **10a**−**c** and NaOH (Scheme 3). [^{11}C]Methylation of **10a**−**c** with [^{11}C]MeI proceeded efficiently for 5 min at 60 °C. HPLC purification of the reaction mixtures gave [^{11}C]**3a** with 31 ± 9% (n = 7), [^{11}C]**3b** with 38 ± 11% (n = 7), and [^{11}C]**3c** with 25 ± 6% (n = 6) radiochemical yields (decay-corrected) based on [^{11}C]CO_2, respectively (Supporting Information: Figure 1). Starting from 11.2−16.3 GBq of [^{11}C]CO_2, 1.2−2.3 GBq of [^{11}C]**3a**−**c** was produced with 22 ± 3 min (n = 20) of synthesis times from the end of bombardment. Identities of these radioactive products were confirmed by coinjection with unlabeled **3a**−**c** on the analytic HPLC chromatograms. In the final formulated solutions, the radiochemical purity of [^{11}C]**3a**−**c** was higher than 99% and specific activity was 70−165 GBq/μmol, as determined by comparison of the assayed radioactivity

Scheme 2. Syntheses of 3a−c[a]

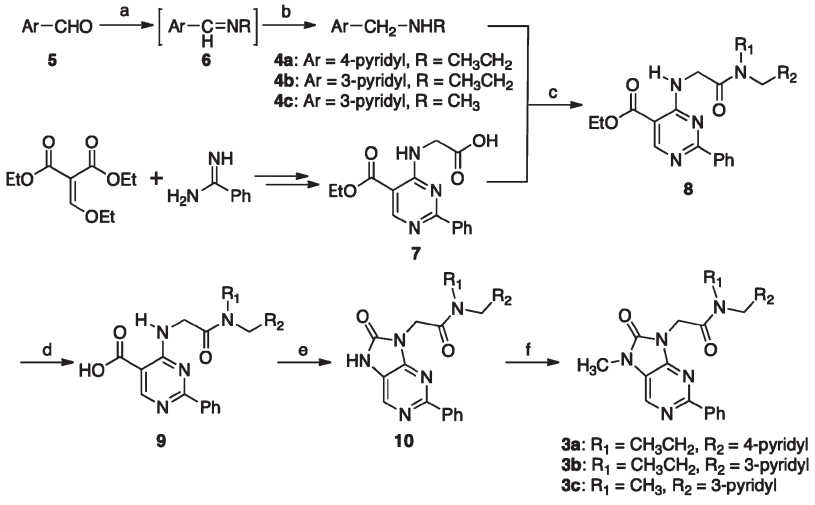

[a] Reagents and conditions: (a) methyl- or ethylamine, ethanol, room temperature, 10 h; (b) $NaBH_4$, ethanol, room temperature, 12 h; (c) BOP, DMF, room temperature, 3 h; (d) NaOH, ethanol, room temperature, 12 h; (e) diphenylphosphoryl azide, Et_3N, DMF, 100 °C, 6 h; (f) MeI, NaH, DMF, 50 °C, 5 h.

dx.doi.org/10.1021/jm200516a |J. Med. Chem. 2011, 54, 6040–6049

Scheme 3. Radiosyntheses of [^{11}C]3a−c[a]

10a: R_1 = CH_3CH_2, R_2 = 4-pyridyl
10b: R_1 = CH_3CH_2, R_2 = 3-pyridyl
10c: R_1 = CH_3, R_2 = 3-pyridyl

[^{11}C]**3a**: R_1 = CH_3CH_2, R_2 = 4-pyridyl
[^{11}C]**3b**: R_1 = CH_3CH_2, R_2 = 3-pyridyl
[^{11}C]**3c**: R_1 = CH_3, R_2 = 3-pyridyl

[a] Reagents and conditions: [^{11}C]MeI, DMF, 60 °C, 5 min.

Table 1. In Vitro Binding Affinity (K_i) for TSPO and Lipophilicity

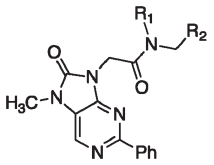

ligand	R_1	R_2	K_i (nM)[a]	cLogD[c]	LogD[b]
3a	CH_3CH_2	4-pyridyl	5.1 ± 0.3	2.38	2.03
3b	CH_3CH_2	3-pyridyl	13.2 ± 0.8	2.38	2.17
3c	CH_3	3-pyridyl	40.0 ± 6.3	1.85	1.81
2			0.6 ± 0.1	3.32	3.48
1			0.7 ± 0.0	5.10	3.74

[a] Values of in vitro binding affinity are the mean ± SD measured in duplicate brain homogenates. [b] cLogD values were calculated with Pallas 3.4 software. [c] LogD values were determined in the octanol/phosphate buffer (pH = 7.40) by the shaking flash method (n = 3; maximum range, ± 5%).

with the mass measured from the carrier UV peak on HPLC (Supporting Information: Figure 2). No significant peaks corresponding to **10a−c** were observed in the HPLC chromatograms of final products. [^{11}C]**3a−c** did not show radiolysis at room temerature for 90 min after formulation, indicating radiochemical stability within the time of at least one PET scan.

In Vitro Binding Assays. In vitro binding affinities (K_i) of **3a−c** for TSPO were measured from competition for the binding of TSPO-selective [^{11}C]**1** using rat brain homogenates. As shown in Table 1, **3a−c** showed high or moderate binding affinity (K_i: 5−40 nM) for TSPO, although the affinity was weaker than those of **1** and **2**. Lower electron density and lipophilicity of the pyridine ring in **3a−c** than those of the benzene ring in **2** may be the main causes of the decrease in the binding affinity for TSPO. The rank order of K_i was **3a** > **3b** > **3c**, suggesting that *N*-ethyl-*N*-(4-pyridylmethyl)amino unity is preferred for binding to TSPO. Because TSPO is present in the lung, heart, and kidney with a high density (B_{max} > 140 pmol/mL),[24] the K_i values of **3a−c** may be enough to elucidate the in vivo specific binding for TSPO in the peripheral organs using PET with [^{11}C]**3a−c**.

Computation and Measurement of Ligand Lipophilicities. The computed values of lipophilicities at pH = 7.4 (cLogD) for [^{11}C]**3a−c** were 1.85−2.38 (Table 1). These values were similar to the corresponding measured values (LogD) of 1.81−2.17, which were measured by the Shake Flask method.[27] The lipophilicity values of [^{11}C]**3a−c** lie in the range normally considered as a favorable PET ligand.[28] The decreased lipophilicity may improve kinetics and reduce nonspecific binding in the targeted regions while performing PET imaging with [^{11}C]**3a−c**.

Small-Animal PET Studies. The in vivo uptake and kinetics in the peripheral organs of rats were examined using small-animal PET with [^{11}C]**3a−c**.

Figure 1 shows the PET summation images between 0 and 30 min after intravenous injection of [^{11}C]**3a** (A), [^{11}C]**3b** (B), or [^{11}C]**3c** (C) in the lung, heart, kidney, liver, and cardiac blood pool of the rat whole body. Higher uptake was found in the lung, heart, and kidney than in the liver. This distribution pattern of radioactivity was consistent with the distribution of TSPO expression in the peripheral organs of rodent animals.[23] As seen in these images, radioactivity also accumulated in the small intestine, suggesting a putative excreting pathway after the radioligands were injected to the rats.

Figure 2 shows the time−activity curves (TACs) in all examined regions of the rat whole body after injection of [^{11}C]**3a** (A), [^{11}C]**3b** (B), or [^{11}C]**3c** (C). The uptake of radioactivity in the heart, lung, and kidney peaked at 1−3 min after injection and then decreased with time in all regions. The radioactivity level in the lung, heart, and kidney decreased from 3.4−5.0 SUV, 4.6−5.5 SUV, and 3.3−4.0 SUV at 2 min to 0.5−0.8 SUV, 0.9−2.0 SUV, and 1.0−2.0 SUV at 27.5 min after injection. On the other hand, uptakes in the cardiac blood pool and liver decreased from 3.0−3.4 SUV and 1.6−2.0 SUV at 2 min after injection to 0.4−0.9 SUV and 0.5−1.2 SUV at the end of PET scans.

For comparison, the TACs in the corresponding regions were determined after injection of [^{11}C]**2** (Figure 2D). The radioactivity in the lung peaked at 1 min (7.6 SUV) after injection and thereafter decreased to 2.3 SUV at 27.5 min. In the heart and kidney, radioactivity peaked at 10 min (heart, 4.2 SUV; kidney, 2.8 SUV), respectively. After the peaked uptake, radioactivity in both organs as well as in the blood and liver remained almost the same level until the end of the PET scans. On the other hand, PET with [^{11}C]**1** showed a similar kinetics to [^{11}C]**2** (Supporting Information: Figure 3).

During the present PET scans, it was found that [^{11}C]**3a−c** displayed improved kinetics in the lung, heart, and kidney in comparison with [^{11}C]**2** and [^{11}C]**1**. This result was partly due to the lower lipophilicity of [^{11}C]**3a−c** (LogD: 1.81−2.17) than [^{11}C]**2** (LogD: 3.48) and [^{11}C]**1** (LogD: 3.74). Introduction of a pyridine ring to [^{11}C]**3a−c** contributed to the decrease in lipophilicity and washout of radioactivity from the lung, heart, and kidney. The rank order of the decreasing rate of radioactivity in these organs after the radioligand injection was [^{11}C]**3a** < [^{11}C]**3b** < [^{11}C]**3c**. Among the three radioligands, [^{11}C]**3a** showed the highest uptake and moderate kinetics in the lung, heart and kidney.

To determine in vivo specific binding for TSPO in the peripheral organs, we performed inhibitory experiments using TSPO-selective ligand **2** or **1**. Figure 3 shows the TACs after injection of [^{11}C]**3a−c** by pretreatment with **2** (A−C) or **1** (D−F) in all regions examined. In the **2**-treated groups as compared to the control, the uptake of radioactivity in the heart, lung, and kidney fell to low levels immediately after injection. Significant inhibition by **1**, a standard TSPO ligand, was also examined in the lung, heart, and kidneys within the PET scans. On the other hand, the liver uptake by treatment with **1** or **2** increased about 1.5-fold, compared to the control at 27.5 min after

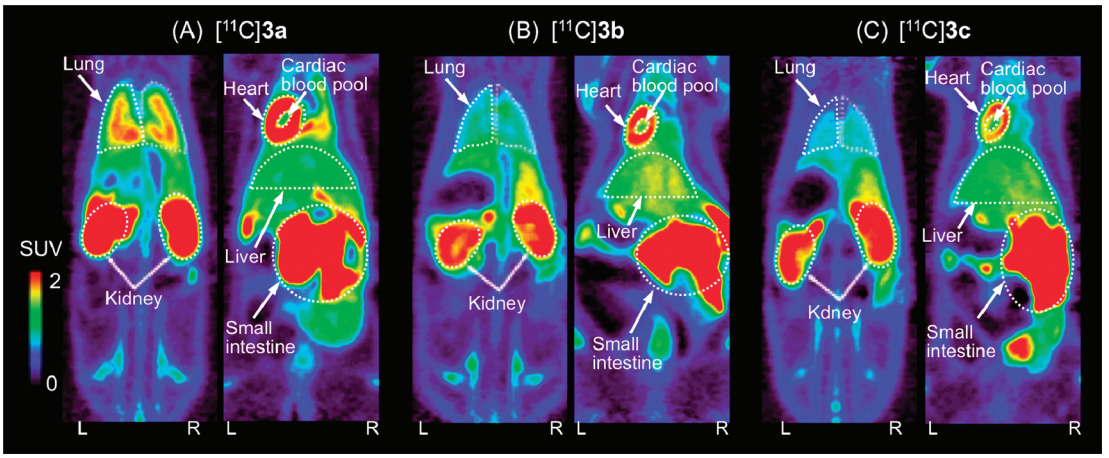

Figure 1. Representative coronal PET images of rat whole body at the levels of the lung, heart, kidney, liver, and cardiac blood pool acquired between 0 and 30 min after intravenous injection of [^{11}C]**3a** ((A) 16 MBq, 0.15 nmol), [^{11}C]**3b** ((B) 17 MBq, 0.18 nmol), and [^{11}C]**3c** ((C) 16 MBq, 0.13 nmol) in the isofurane-anesthetized rat, which was placed in the prone position. L and R indicate left and right side of the rats.

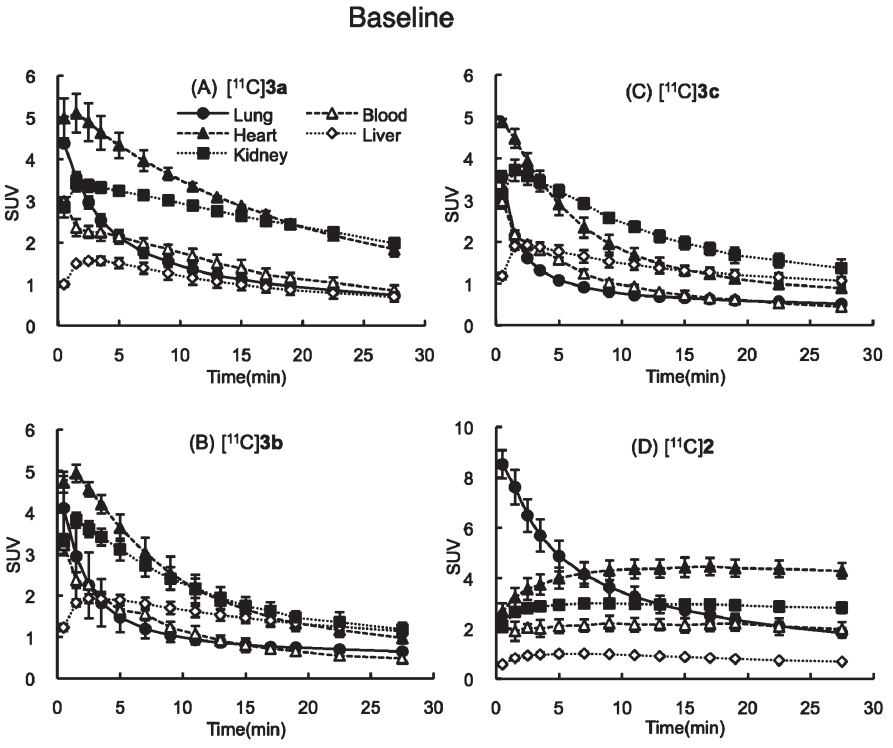

Figure 2. Time−activity curves in the isoflurane anesthetized rat lung (●), heart (▲), kidney (■), liver (◇), and cardiac blood pool (△) after intravenous injection of [^{11}C]**3a** (A), [^{11}C]**3b** (B), [^{11}C]**3c** (C), and [^{11}C]**2** (D). PET scans were performed for 30 min after the injection of each radioligand. Data are the means ± SD (n = 4).

injection. The increased liver uptake may be due to displacement of specially bound radioligand from heart, lung, kidney, etc., by **1** and **2**.

The maximum inhibitory percentages accounting for total uptakes in the organs by treatment with **2** or **1** during PET scans with [^{11}C]**3a**−**c** were calculated (Supporting Information: Table 1). High inhibitory percentages were determined in the lung (66−85%), heart (80−92%), and kidney (55−74%). These results indicated the presence of high in vivo specific binding for TSPO in the peripheral organs. The rank order of specific binding for TSPO in these organs was [^{11}C]**3a** > [^{11}C]**3b** > [^{11}C]**3c**. The in vivo specific binding level of [^{11}C]**3a**−**c** for TSPO was proportional to the sequence of their in vitro binding affinity (Table 1). Among the three radioligands, [^{11}C]**3a**, showing the highest binding affinity for TSPO, exhibited the highest in vivo specific binding for TSPO in the peripheral organs. Because of its in vitro binding affinity, kinetics, and in vivo specific binding, [^{11}C]**3a** was selected for further investigation.

Metabolite Analysis. In the imaging study, the presence of significant quantities of radiolabeled metabolites in the target

dx.doi.org/10.1021/jm200516a |*J. Med. Chem.* 2011, 54, 6040–6049

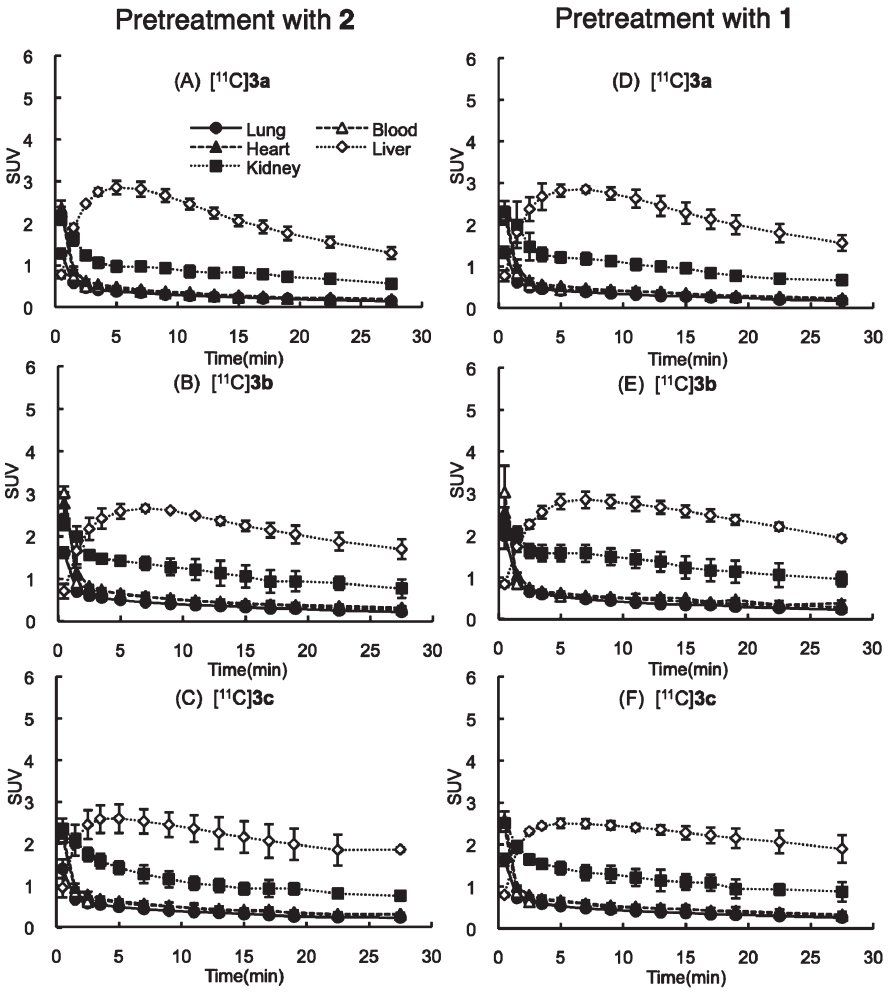

Figure 3. Time−activity curves in the isoflurane anesthetized rat lung (●), heart (▲), kidney (■), liver (◇), and cardiac blood pool (△) after intravenous injection of [^{11}C]**3a** (A,D), [^{11}C]**3b** (B,E), and [^{11}C]**3c** (C,F) in pretreatment experiments, in which unlabeled **2** (1 mg/kg, A−C) or **1** (3 mg/kg, D−F) was given at 1 min before radioligand. PET scans were performed for 30 min after the injection of each radioligand. Data are the means ± SD (n = 4).

tissues may produce an insurmountable barrier to the proper quantification of images and interpretation of the results. Here, we performed metabolite analysis in the plasma, heart, lung, liver, and kidney of rats at 30 min after injection of [^{11}C]**3a**.

Table 2 shows the percentages of unchanged [^{11}C]**3a** (retention time (t_R): 7.8 min) in these tissues, as determined by analytical radio-HPLC. In addition to the unchanged [^{11}C]**3a**, a polar radioactive peak (t_R: 2.6 min) corresponding to a radiolabeled metabolite appeared on the front line of HPLC chromatograms of the plasma and liver. On the other hand, more than 90% of the total radioactive component was identified as the unchanged [^{11}C]**3a** in the lung, heart, and kidney at 30 min after injection, respectively. This result indicated that despite the presence of radiolabeled metabolite in the plasma and liver, the specific binding for TSPO examined in the lung, heart, and kidney was mainly due to [^{11}C]**3a** itself and was not influenced by the radiolabeled metabolite. This finding further supported that [^{11}C]**3a** is a potent PET ligand for imaging TSPO in the lung, heart, and kidney.

Visualization of Lung Inflammation. To elucidate the usefulness of [^{11}C]**3a** for imaging inflammation in the peripheral organs, we performed PET study with [^{11}C]**3a** using a rat model of lung inflammation. By injecting LPS (5 mg/kg) intratracheally to rats, inflammation was induced in the lungs.[29,30] It has been reported that TSPO expression was augmented in the lungs of the LPS-treated rats, although the cellular sources enriching TSPO expression in the lung have not been determined clearly.[30,31]

Figure 4 shows representative PET summation images of LPS-treated (A) and control (vehicle) (B) rat lungs between 0 and

Table 2. Percentages of Unchanged [^{11}C]3a in the Plasma and Peripheral Tissues of Rats at 30 min after Injection[a]

tissue	% of unchanged [^{11}C]**3a**
plasma	23.4 ± 0.8
liver	43.6 ± 1.2
lung	92.1 ± 2.2
heart	93.8 ± 1.4
kidney	94.7 ± 3.5

[a] Data are the means of ± SD (n = 3) in each tissue.

dx.doi.org/10.1021/jm200516a |J. Med. Chem. 2011, 54, 6040–6049

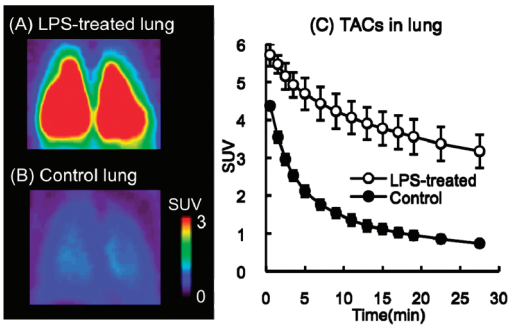

Figure 4. Representative coronal PET images of LPS-treated (A) and control (B) lungs acquired between 0 and 30 min after intravenous injection of [^{11}C]**3a** (17 MBq, 0.15 nmol). Time−activity curves (C) were obtained in LPS-treated (○) and control (●) lung of inflammatory rats after injection of [^{11}C]**3a**. Data are the means ± SD (n = 4).

Table 3. Biodistribution (% ID/g Tissue: mean ± SD, n = 4) in Rats after Injection of [^{11}C]3a

tissue	control	LPS-treated
blood	0.06 ± 0.00	0.08 ± 0.01
brain	0.02 ± 0.00	0.02 ± 0.00
lung	1.65 ± 0.12	3.54 ± 0.73
heart	2.10 ± 0.22	2.17 ± 0.17
liver	0.53 ± 0.04	1.03 ± 0.28
kidney	1.78 ± 0.12	1.97 ± 0.15
spleen	1.88 ± 0.16	1.88 ± 0.37
pancreas	0.38 ± 0.04	0.37 ± 0.07
adrenal	7.49 ± 2.55	5.27 ± 1.32
small intestine	1.57 ± 0.46	2.68 ± 1.36
muscle	0.11 ± 0.03	0.10 ± 0.01

30 min after injection of [^{11}C]**3a**. The accumulation of radioactivity was observed in the lungs of LPS-treated rats, whereas no such accumulation was found in the lungs of control rats. Differences in the TACs were significant between LPS-treated and control lungs (Figure 4C). As calculated from the TACs, the values of area under TACs between 0 and 30 min ($AUC_{0-30\ min}$ = SUV × min) in the lungs were 43.5 ± 3.5 for the control and 118.6 ± 11.5 for the LPS-treated rats, respectively. On the other hand, the corresponding values of $AUC_{0-30\ min}$ in the lungs for [^{11}C]**1** were 62.8 ± 4.0 for the control and 86.0 ± 2.4 for the LPS-treated rats, respectively (Supporting Information: Figure 4).

To support the present PET results, the radioactivity concentrations were measured in the control and LPS-treated rats by the dissection method. Table 3 shows the radioactivity in various tissues of two groups of rats at 30 min after injection of [^{11}C]**3a**. The radioactivity level in LPS-treated lungs was 2.1-fold higher than that in control lungs, which was similar to the PET result. In addition to the lungs, increased radioactivity was seen in the liver and small intestine. No significant difference in uptake in the other regions was determined between the control and LPS-treated rats. PET study with [^{11}C]**3a** for LPS-treated rats showed that radioactivity increased in the lung in response to lung inflammation. Radioactive signals in LPS-treated lungs may be due to the increase in TSPO expression compared to the control lungs.

SUMMARY

To visualize TSPO in the peripheral organs and lung inflammation, three novel oxopurine analogues **3a**−**c** were developed and labeled with ^{11}C. [^{11}C]**3a**−**c** were synthesized by [^{11}C]-methylation of the desmethyl precursor **10a**−**c** with [^{11}C]MeI in high radiochemical yields. Compounds **3a**−**c** exhibited high or moderate in vitro binding affinity (K_i: 4−50 nM) with TSPO and suitable lipophilicity (LogD: 1.81−2.17) as a favorable PET ligand. Compared to lead compound [^{11}C]**2**, PET with [^{11}C]-**3a**−**c** demonstrated that the kinetics in the lung, heart, and kidney of rats had improved. Among the three radioligands, [^{11}C]**3a** had the highest in vitro binding affinity for TSPO, uptake, and in vivo specific binding and displayed moderate kinetics in the lung, heart, and kidney. Only unchanged [^{11}C]**3a** was found in these organs despite the presence of radiolabeled metabolite in the plasma and liver at 30 min after the radioligand injection.

PET with [^{11}C]**3a** provided an observatory signal in the lung of LPS-treated rats. Thus, [^{11}C]**3a** may be a useful PET ligand for the visualization of TSPO-related disease such as inflammation. Because of the suitable kinetics, the utilization of PET with [^{11}C]**3a** would contribute to the study of TSPO function and quantitative evaluation of in vivo binding parameters and receptor occupancy of TSPO therapeutic compounds.

EXPERIMENTAL SECTION

Materials and Methods. All chemical reagents and solvents were purchased from commercial sources (Sigma-Aldrich, MO; Wako Pure Chemical Industries, Osaka, Japan; Tokyo Chemical Industries, Tokyo, Japan) and used as supplied. Compound **1** was purchased from Tocris Bioscience (Bristol, UK) and **2** was prepared in our laboratory.[17] ^{1}H NMR (300 MHz) spectra were recorded on a JEOL-AL-300 spectrometer (JEOL, Tokyo) with tetramethylsilane as an internal standard. All chemical shifts (δ) were reported in parts per million (ppm) downfield relative to the chemical shift of tetramethylsilane. Signals are quoted as s (singlet), d (doublet), dd (double doublet), dt (double triplet), dq (double quartet), t (triplet), q (quartet), or m (multiplet). Fast atom bombardment mass spectra (FAB-MS) and high-resolution mass spectra (HRMS) were obtained on a JEOL-NMS-SX102 spectrometer (JEOL) and recorded on the spectrometer. Melting points were measured using a micro melting point apparatus (MP-500P, Yanaco, Tokyo) and are uncorrected. Column chromatography was performed using Wako gel C-200 (70−230 mesh). High performance liquid chromatography (HPLC) was performed using a JASCO HPLC system (JASCO, Tokyo). Chemical purity (≥95%) of compounds was assayed by analytical HPLC (**10**: Capcell Pack C_{18}, 4.6 mm ID × 250 mm, UV at 254 nm, MeCN/H_2O 4/6. **3**: Capcell Pack C_{18}, 4.6 mm ID × 250 mm, UV at 254 nm, MeCN/H_2O 4.5/5.5.). Carbon-11 (^{11}C) was produced by the ^{14}N (p,α) ^{11}C nuclear reaction using a CYPRIS HM-18 cyclotron (Sumitomo Heavy Industry, Tokyo). If not otherwise stated, radioactivity was measured with an IGC-3R Curiemeter (Aloka, Tokyo). Radioligands [^{11}C]**1** and [^{11}C]**2** were synthesized according to the procedures described previously.[10,17] In radio-HPLC purifiaction and analysis, effluent radioactivity was monitored using a NaI (Tl) scintillation detector system.

Chemistry. *N-Ethyl-4-pyridylmethylamine (**4a**).* A mixture of 4-pyridinecarboxaldehyde (**5a**; 1.52 g, 10 mmol) and ethylamine (3 mL) in ethanol (5 mL) was stirred for 10 h at room temperature. After the reaction, $NaBH_4$ (0.38 g, 10 mmol) was added to this mixture. The reaction mixture was continuously stirred at room temperature for 12 h and then evaporated in vacuo to remove ethanol. The residue was extracted with dichloromethane (CH_2Cl_2) and water, and the organic

layer was dried over Na_2SO_4 and evaporated. The crude product was purified by silica gel column chromatography (CH_2Cl_2/methanol: 10/1) to give **4a** (2.30 g, 70.6%) as a colorless liquid. ^{1}H NMR ($CDCl_3$, δ): 8.54 (2H, d, J = 4.4 Hz), 7.26 (2H, d, J = 5.1 Hz), 3.81 (2H, s), 2.68 (2H, q, J = 7.0 Hz), 1.14 (3H, t, J = 7.0 Hz). FAB−MS: m/z 137 (M + H).

*N-Ethyl-3-pyridylmethylamine (**4b**).* The procedure described for the synthesis of **4a** was applied to 3-pyridinecarboxaldehyde (**5b**) and ethylamine to give **4b** (73.4%) as a colorless liquid. ^{1}H NMR ($CDCl_3$, δ): 8.56 (1H, s), 8.50 (1H, d, J = 3.7 Hz), 7.68 (1H, d, J = 7.7 Hz), 7.23−7.30 (1H, m), 3.81 (2H, s), 2.69 (2H, q, J = 7.0 Hz), 1.14 (3H, t, J = 7.0 Hz). FAB−MS: m/z 137 (M + H).

*N-Methyl-3-pyridylmethylamine (**4c**).* The procedure described for the synthesis of **4a** was applied to **5b** and methylamine to give **4c** (66.3%) as a colorless liquid. ^{1}H NMR ($CDCl_3$, δ): 8.55−8.56 (1H, m), 8.51 (1H, dd, J = 1.5, 4.0 Hz) 7.67−7.70 (1H, m), 7.25−7.29 (1H, m), 3.77 (2H, s), 2.46 (3H, s), 1.99 (1H, s). FAB−MS: m/z 123 (M + H).

*Ethyl 4-(2-(N-Ethyl,N-4-pyridylmethylamino)-2-oxoethylamino-2-phenylpyrimidine-5-carboxylate (**8a**).* The BOP reagent (2.00 g, 4.4 mmol) was added to a mixture of 2-(5-ethoxycarbonyl)-2-phenylpyrimidine-4-ylamino)acetic acid[24] (**7**; (1.20 g, 4.0 mmol), Et_3N (0.61 mL, 4.4 mmol) and **4a** (0.62 g, 4.5 mmol) in DMF (25 mL). The reaction mixture was stirred at room temperature for 3 h and then evaporated in vacuo to remove DMF. The residue was extracted with ethyl acetate and water, and the organic layer was dried over Na_2SO_4 and evaporated. The crude product was purified by open column chromatography (*n*-hexane/ethyl acetate: 2/1) to give **8a** (0.73 g, 38.5%) as a colorless solid; mp 124−126 °C. ^{1}H NMR ($CDCl_3$, δ): 9.00 (1H, s), 8.39−8.46 (4H, m), 7.79 (1H, dd, J = 8.1, 59.0 Hz), 7.24−7.49 (5H, m), 4.68 (2H, d, J = 12.8 Hz), 4.57 (2H, d, J = 4.8 Hz), 4.41 (2H, q, J = 7.1 Hz), 3.27 (2H, q, J = 7.3 Hz), 1.34−1.44 (6H, m). FAB−MS: m/z 420 (M + H).

*Ethyl 4-(2-(N-Ethyl,N-3-pyridylmethylamino)-2-oxoethylamino-2-phenylpyrimidine-5-carboxylate (**8b**).* The procedure described for the synthesis of **8a** was applied to **7** and **4b** to give **8b** (19.0%) as a colorless solid; mp 121−122 °C. ^{1}H NMR ($CDCl_3$, δ): 8.95−9.01 (2H, m), 8.50−8.59 (2H, m), 8.34 (2H, dd, J = 6.4, 25.5 Hz), 7.58−7.68 (1H, m), 7.45−7.50 (3H, m), 7.15−7.19 (1H, m), 4.67 (2H, d, J = 6.6 Hz), 4.48 (2H, dd, J = 4.4, 13.6 Hz), 4.41 (2H, q, J = 7.2 Hz), 3.39−3.53 (2H, m), 1.15−1.44 (6H, m). FAB−MS: m/z 420 (M + H).

*Ethyl 4-(2-(N-Methyl,N-3-pyridylmethylamino)-2-oxoethylamino-2-phenylpyrimidine-5-carboxylate (**8c**).* The procedure described for the synthesis of **8a** was applied to **7** and **4c** to give **8c** (46.9%) as a colorless solid; mp 136−137 °C. ^{1}H NMR ($CDCl_3$, δ): 8.96−9.04 (2H, m), 8.53−8.61 (2H,m), 8.31−8.46 (2H, m), 7.45−7.68 (4H, m), 7.19−7.32 (1H, m), 4.67 (2H, d, J = 7.3 Hz), 4.48−4.57 (2H, m), 4.40 (2H, q, J = 7.1 Hz), 3.09 (3H, s), 1.42 (3H, t, J = 7.1 Hz). FAB−MS: m/z 406 (M + H).

*4-(2-(N-Ethyl,N-4-pyridylmethylamino)-2-oxoethylamino-2-phenylpyrimidine-5-carboxylic Acid (**9a**).* A mixture of **8a** (0.71 g, 1.7 mmol) and NaOH (1 mL, 5 M) in ethanol (50 mL) was stirred at room temperature for 12 h. After ethanol was removed, HCl (1 M) was added slowly to neutralize the reaction mixture. The obtained precipitate was collected and washed with water to give **10a** (80.1%) as a colorless solid; mp 244−245 °C. ^{1}H NMR (DMSO-d_6, δ): 13.4 (1H, br), 8.83−8.87 (2H, m), 8.23−8.66 (3H, m), 7.48−7.57 (5H, m), 4.68 (2H, s), 4.55 (2H, dd, J = 5.3, 77.2 Hz), 3.48 (2H, dq, J =7.0, 33.4 Hz), 1.16 (3H, dt, J = 7.0, 47.4 Hz). FAB−MS: m/z 392 (M + H).

*4-(2-(N-Ethyl,N-3-pyridylmethylamino)-2-oxoethylamino-2-phenylpyrimidine-5-carboxylic Acid (**9b**).* The procedure described for the synthesis of **9a** was applied to **8b** to give **9b** (98.4%) as a colorless solid; mp 163−164 °C. ^{1}H NMR (DMSO-d_6, δ): 8.86 (2H, t, J = 7.9 Hz), 8.52−8.67 (2H, m), 8.35 (2H, dd, J = 7.2, 26.6 Hz), 7.85−7.92 (1H, m), 7.37−7.56 (4H, m), 4.50−4.78 (4H, m), 3.38−3.50 (2H, m), 1.13 (3H, dt, J = 7.0, 55.7 Hz). FAB−MS: m/z 392 (M + H).

*4-(2-(N-Methyl,N-3-pyridylmethylamino)-2-oxoethylamino-2-phenylpyrimidine-5-carboxylic Acid (**9c**).* The procedure described for the synthesis of **9a** was applied to **8c** to give **9c** (68.5%) as a colorless solid; mp 154−155 °C. ^{1}H NMR (DMSO-d_6, δ): 8.96−9.04 (2H, m), 8.53−8.61 (2H,m), 8.31−8.46 (2H, m), 7.45−7.68 (4H, m), 7.19−7.32 (1H, m), 4.67 (2H, d, J = 7.3 Hz), 4.48−4.57 (2H, m), 4.40 (2H, q, J = 7.1 Hz), 3.09 (3H, s), 1.42 (3H, t, J = 7.1 Hz). FAB−MS: m/z 378 (M + H).

*N-Ethyl-N-(4-pyridylmethyl)-2-(8-oxo-2-phenyl-7,8-dihydro-9H-purin-9-yl)acetamide (**10a**).* Diphenylphosphoryl azide (0.22 mL, 1 mmol) was added to a solution of **9a** (0.39 g, 1 mmol) and triethylamine (Et_3N; 0.14 mL, 1 mmol) in DMF (5 mL). The reaction mixture was heated at 100 °C for 6 h and then evaporated to remove DMF. The residue was extracted with ethyl acetate, and the organic layer was washed with brine and dried over Na_2SO_4. After the solvent was removed, the crude product was purified by column chromatography (CH_2Cl_2/methanol: 95/0.5) and recrystallized from methanol to give **10a** (0.18 g, 46.9%) as colorless solid; mp 212−213 °C. ^{1}H NMR (DMSO-d_6, δ): 11.50 (1H, s), 8.65 (1H, d, J = 5.9 Hz), 8.27−8.38 (4H, m), 7.41−7.52 (4H, m), 7.22 (1H, d, J = 5.5 Hz), 4.56−4.96 (4H, m), 3.47 (2H, dq, J = 7.0, 71.7 Hz), 1.16 (3H, dt, J = 7.0, 68.9 Hz). HRMS (FAB) calcd for $C_{21}H_{20}N_6O_2$, 389.1726; found, 389.1757.

*N-Ethyl-N-(3-pyridylmethyl)-2-(8-oxo-2-phenyl-7,8-dihydro-9H-purin-9-yl)acetamide (**10b**).* The procedure described for the synthesis of **10a** was applied to **9b** to give **10b** (73.1%) as a colorless solid; mp 203−204 °C. ^{1}H NMR (DMSO-d_6, δ): 9.87 (1H, s), 8.49−8.66 (2H, m), 8.31 (2H, d, J = 3.7 Hz), 8.14 (1H, d, J = 8.5 Hz), 7.39−7.64 (4H, m), 7.11 (1H, m), 4.63−4.87 (4H, m), 3.47 (2H, d, J = 6.2 Hz), 1.11−1.38 (3H, m). HRMS (FAB) calcd for $C_{21}H_{20}N_6O_2$, 389.1726; found, 389.1757.

*N-Methyl-N-(3-pyridylmethyl)-2-(8-oxo-2-phenyl-7,8-dihydro-9H-purin-9-yl)acetamide (**10c**).* The procedure described for the synthesis of **10a** was applied to **9c** to give **10c** (73.4%) as a colorless solid; mp 206−207 °C. ^{1}H NMR (DMSO-d_6, δ): 11.53 (1H, s), 8.57−8.62 (1H, m), 8.47−8.49 (1H, m), 8.29−8.38 (2H, m), 7.62−7.87 (1H, m), 7.48−7.52 (2H, m), 7.13−7.32 (3H, m), 4.57−4.92 (4H, m), 3.25 (3H, d, J = 46.6 Hz). HRMS (FAB) calcd for $C_{20}H_{18}N_6O_2$, 375.1569; found, 375.1599.

*N-Ethyl-N-(4-pyridylmethyl)-2-(7-methyl-8-oxo-2-phenyl-7,8-dihydro-9H-purin-9-yl)acetamide (**3a**).* A mixture of **10a** (72 mg, 0.18 mmol), MeI (13 μL, 0.21 mmol) and sodium hydride (NaH; 60% in mineral oil, 9 mg, 0.24 mmol) in DMF (1 mL) was stirred at 50 °C for 5 h. After DMF was removed on reduced pressure, the residue was quenched with ethyl acetate and washed with water and a saturated NaCl solution. After the organic layer was dried over Na_2SO_4, the solvent was removed to give a crude product, which was recrystallized from methanol to give **3a** (0.99 g, 33.3%) as a colorless solid; mp 184−185 °C. ^{1}H NMR (DMSO-d_6, δ): 8.54−8.66 (2H, m), 8.28−8.37 (3H, m), 7.40−7.50 (4H, m), 7.22 (1H, d, J = 5.1 Hz), 4.50−5.01 (4H, m), 3.15 (3H, d, J = 5.1 Hz), 3.45 (2H, dq, J = 7.0, 73.1 Hz), 3.15 (3H, d, J = 5.1 Hz), 1.12 (3H, dt, J = 7.0, 70.4 Hz). HRMS (FAB) calcd for $C_{22}H_{22}N_6O_2$, 403.1862; found, 403.1836.

*N-Ethyl-N-(3-pyridylmethyl)-2-(7-methyl-8-oxo-2-phenyl-7,8-dihydro-9H-purin-9-yl)acetamide (**3b**).* The procedure described for the synthesis of **3a** was applied to **10b** to give **3b** (49.2%) as a colorless solid; mp 185−187 °C. ^{1}H NMR (DMSO-d_6, δ): 8.64 (1H, s), 8.52 (1H, s), 8.24−8.36 (3H, m), 7.72 (1H, dd, J = 7.9, 52.2 Hz), 7.38−7.46 (3H, m), 7.12−7.17 (1H, m), 4.88 (2H, d, J = 18.0 Hz), 4.66 (2H, d, J = 22.0 Hz), 3.45−3.52 (5H, m), 1.27 (3H, dt, J = 7.2, 69.3 Hz. HRMS (FAB) calcd for $C_{22}H_{20}N_6O_2$, 403.1862; found, 403.1836.

*N-Methyl-N-(3-pyridylmethyl)-2-(7-methyl-8-oxo-2-phenyl-7,8-dihydro-9H-purin-9-yl)acetamide (**3c**).* The procedure described for the synthesis of **3a** was applied to **10c** to give **3c** (54.6%) as a colorless solid; mp 171−172 °C. ^{1}H NMR (DMSO-d_6, δ): 8.53−8.67 (2H, m), 8.25−8.36 (3H, m), 7.62−7.78 (1H, m), 7.38−7.46 (3H, m), 7.18−7.23 (1H, m), 4.90 (2H, d, J = 8.8 Hz), 4.66 (2H, d, J = 23.8 Hz), 3.50 (3H, s), 2.99 (3H, s). HRMS (FAB) calcd for $C_{21}H_{22}N_6O_2$, 389.1726; found, 389.1757.

Radiochemistry. *N-Ethyl-N-(4-pyridinylmethyl)-2-(7-[^{11}C]methyl-8-oxo-2-phenyl-7,8-dihydro-9H-purin-9-yl)acetamide ([^{11}C]**3a**).* [^{11}C]MeI for labeling was synthesized from cyclotron-produced [^{11}C]CO_2 as described previously.[26] Briefly, [^{11}C]CO_2 was bubbled into 0.4 M $LiAlH_4$ in anhydrous tetrahydrofuran (THF, 300 μL). After evaporation of THF, the remaining complex was treated with 57% hydroiodic acid (300 μL). The produced [^{11}C]MeI was transferred under helium gas flow with heating into a reaction vessel containing desmethyl precursor **10a** (0.6−0.8 mg), NaOH (3−5 μL, 0.1 M), and anhydrous DMF (300 μL) cooled to −15 to −20 °C. After radioactivity reached a plateau, the reaction vessel was warmed to 60 °C and maintained for 5 min. MeCN/H_2O (4/6, 500 μL) was added to the reaction mixture to stop the reaction, and the mixture was applied to the semipreparative HPLC system. HPLC purification was completed on a Capcell Pack C_{18} column (10 mm ID × 250 mm; Shiseido, Tokyo) using a mobile phase of MeCN/H_2O (4/6) at a flow rate of 5.0 mL/min. The t_R for [^{11}C]**3a** was 8.0 min, whereas that for unreacted **10a** was 4.9 min. The radioactive fraction corresponding to the desire product was collected in a sterile flask, evaporated to dryness in vacuo, redissolved in 3 mL of sterile normal saline, and passed through a 0.22 μm Millipore filter for analysis and animal experiments. The synthesis time was 23 min from the end of bombardment.

Radiochemical purity was assayed by analytical HPLC (Capcell Pack C_{18}, 4.6 mm ID × 250 mm, UV at 254 nm; MeCN/H_2O, 4/6; t_R, 7.8 min). The identity of [^{11}C]**3a** was confirmed by coinjection with unlabeled **3a**. The specific activity of [^{11}C]**3a** was calculated by comparison of the assayed radioactivity to the mass associated with the carrier UV peak at 254 nm. Radiochemical yield (decay-corrected), 35% based on [^{11}C]CO_2; radiochemical purity, >99%; specific activity, 100 GBq/μmol.

*N-Ethyl-N-(3-pyridinylmethyl)-2-(7-[^{11}C]methyl-8-oxo-2-phenyl-7,8-dihydro-9H-purin-9-yl)acetamide ([^{11}C]**3b**).* The procedure described for the synthesis of [^{11}C]**3a** was applied to **10b** to give [^{11}C]**3b**; t_R, 8.3 min for purification and 8.0 min for analysis; synthesis time, 24 min; radiochemical yield (decay-corrected), 34% based on total [^{11}C]CO_2; radiochemical purity, >99%; specific activity, 106 GBq/μmol.

*N-Methyl-N-(3-pyridinylmethyl)-2-(7-[^{11}C]methyl-8-oxo-2-phenyl-7,8-dihydro-9H-purin-9-yl)acetamide ([^{11}C]**3c**).* The procedure described for the synthesis of [^{11}C]**3a** was applied to **10c** to give [^{11}C]**3c**; t_R, 8.1 min for purification and 6.2 min for analysis; synthesis time, 22 min; radiochemical yield (decay-corrected), 23% based on total [^{11}C]CO_2; radiochemical purity, > 99%; specific activity, 98 GBq/μmol.

Measurement and Computation of Lipophilicity. The LogD values were measured by mixing [^{11}C]**3a**−**c** (radiochemical purity, 100%; about 200000 cpm) with *n*-octanol (3.0 g) and sodium phosphate buffer (PBS; 3.0 g, 0.1 M, pH 7.4) in a test tube. The tube was vortexed for 3 min at room temperature, followed by centrifugation at 3500 rpm for 5 min. An aliquot of 1 mL PBS and 1 mL *n*-octanol was removed, weighted, and counted, respectively. Samples from the remaining organic layer were removed and repartitioned until consistent LogD values were obtained. The LogD value was calculated by comparing the ratio of cpm/g of *n*-octanol to that of PBS and expressed as LogD = Log[cpm/g (*n*-octanol)/cpm/g (PBS)]. All assays were performed in triplicate. Meanwhile, the values of cLogD of [^{11}C]**3a**−**c** were computed using Pallas 3.4 software (CompuDrug, Sedona, AZ).

Evaluation. Male Sprague−Dawley rats (6−8 weeks old) were purchased from Japan SLC (Shizuoka, Japan). The rats were housed under a 12-h dark−light cycle and were allowed free access to food pellets and water. The animal experiments were approved by the Animal Ethics Committee of the National Institute of Radiological Sciences (Chiba, Japan).

In Vitro Binding Assays for TSPO. For this assay, the method described previously was used.[32] Rats (n = 5) were sacrificed by decapitation under ether anesthesia. The whole brains were rapidly dissected and homogenized in 10 volumes of ice-cold Tris-HCl buffer (10 mM, pH 7.4, containing 320 μM sucrose). The homogenate was centrifuged at 77*g* for 10 min at 4 °C. The supernatant was collected and then centrifuged at 9000*g* for 10 min at 4 °C. The pellet was suspended in Tris-HCl buffer (10 mM, pH 7.4, containing 320 μM sucrose) and centrifuged at 9000*g* for 10 min at 4 °C. The resulting pellet was then washed with 50 mM Tris-HCl buffer (pH 7.4) by centrifugation at 12000*g* for 10 min at 4 °C. Finally, the crude mitochondrial pellet was resuspended in 50 mM Tris-HCl buffer (pH 7.4) at a concentration of 100 μg original wet tissue/mL and used for binding assays.

Each crude mitochondrial preparation (100 μL) was incubated with [^{11}C]**1** (final concentration 3.4 ± 0.6 nM) and various concentrations of tested ligands (**1**, **2**, **3a**−**c**) in a total volume of 1 mL at room temperature for 30 min, and the reaction was terminated by rapid filtration through 0.3% polyethylenimine-pretreated Whatman GF/C glass fiber filters, using a cell harvester (M-24, Brandel, Gaithersburg, MD). The filters were immediately washed three times with 5 mL of ice-cold Tris-HCl buffer (50 mM), and the filter-bound radioactivity was quantified using a γ counter (Wallac 1470 WIZARD 3″, PerkinElmer, Waltham, MA). Nonspecific binding was determined in the presence of **1** (10 μM). All assays were performed in duplicate, except for total binding and nonspecific binding, which were in quadruplicate. Specific binding at each compound concentration was calculated as a percentage in relation to the control specific binding, and which were converted to probit values to determine the IC_{50} of each compound. The IC_{50} value was further converted to K_i according to the Cheng−Prusoff equation.[33]

PET Studies on Normal Rats. PET scans were performed using a small-animal Inveon PET scanner (Siemens Medical Solutions USA, Knoxville, TN), which provides 159 transaxial slices 0.796 mm (center-to-center) apart, a 10 cm transaxial field of view (FOV), and a 12.7 cm axial FOV. Before scans, the rats were anesthetized with 5% (v/v) isoflurane and maintained thereafter by 1−2% (v/v) isoflurane. Emission scans were acquired for 30 min in three-dimensional list mode with an energy window of 350−750 keV, immediately after intravenous injection of [^{11}C]**3a**−**c** (16−18 MBq/200 μL, 0.13−0.24 nmol). To determine in vivo specific binding, unlabeled **1** (3.0 mg/kg) and **2** (1.0 mg/kg dissolved in 300 μL saline containing 10% ethanol and 5% polysorbate 80) were injected at 1 min before injection of [^{11}C]**3a**−**c**. Four rats were used for each experiment. All list-mode acquisition data were sorted into three-dimensional sinograms, which were then Fourier rebinned into two-dimensional sinograms (frames × min: 2 × 2, 1 × 4, 4 × 5). Dynamic images were reconstructed with filtered back-projection using a Hanning's filter, with a Nyquist cutoff of 0.5 cycle/pixel. Regions of interest were placed on the lung, heart, kidney, liver, small intestine, and cardiac blood pool using ASIPro VM (Analysis Tools and System Setup/Diagnostics Tool, Siemens Medical Solutions USA). Regional uptake of radioactivity was decay-corrected to the injection time and was expressed as the standardized uptake value (SUV), which was normalized to the injected radioactivity and body weight. SUV = (radioactivity per mL tissue/injected radioactivity) × g body weight. For comparison, PET with [^{11}C]**1** and [^{11}C]**2** (15−20 MBq/200 μL, 0.15−0.18 nmol) was performed according to the same procedures described above.

Metabolite Assay for Rat Tissue. After intravenous injection of [^{11}C]**3a** (37 MBq/100 μL, 0.32 nmol) into rats (n = 3), these rats were sacrificed by cervical dislocation at 30 min. Blood (0.7−1.0 mL), lung, heart, liver, and kidney samples (0.5−1.0 g) were removed quickly. The blood sample was centrifuged at 15000 rpm for 1 min at 4 °C to separate plasma, and 250 μL of plasma was collected in a test tube containing MeCN (500 μL) and a solution of the authentic unlabeled **3a** (0.5 mg/5.0 mL MeCN, 10 μL). After the tube was vortexed for 15 s and centrifuged at 15000 rpm for 2 min for deproteinization, the supernatant was collected. The extraction efficiency of radioactivity into the MeCN supernatant ranged from 81% to 95% of the total radioactivity in the plasma. On the other hand, the lung, heart, kidney, and liver were dissected and homogenized together in an ice-cooled MeCN/H_2O (4/6, 1.0 mL) solution. The homogenate was centrifuged at 15000 rpm for 1 min at 4 °C

and supernatant was collected. The recovery of radioactivity into the supernatant was 71−85% based on the total radioactivity in the tissue homogenate.

An aliquot of the supernatant (100−500 μL) obtained from the plasma or tissue homogenate was injected into the HPLC system for radioactivity and analyzed under the same conditions described above. The percent ratio of [^{11}C]**3a** (t_R, 7.8 min) to total radioactivity (corrected for decay) on the HPLC chromatogram was calculated as % = (peak area for [^{11}C]**3a**/total peak areas) × 100.

Preparation of Rat Model of Lung Inflammation. Rats were intratracheally injected with lipopolysaccharide (LPS, *Escherichia coli* O127, B8, Sigma-Aldrich; about 125 μg in 50 μL saline, 5.0 mg/kg), respectively. Control (vehicle) rats received treatment with 50 μL of saline. Twenty-four hours after LPS treatment or control, these rats were used for PET and biodistribution studies.

PET Study on LPS-Treated Rats. PET scans with [^{11}C]**3a** and [^{11}C]**1** (15−17 MBq/200 μL, 0.15−0.17 nmol) were performed for control and LPS-treated rats according to the same procedures described for normal rats.

Biodistribution in LPS-Treated Rats by Dissection. A saline solution of [^{11}C]**3a** (16 MBq/200 μL, 0.19 nmol) was injected into LPS-treated and vehicle rats through the tail vein. Four rats for each group were sacrificed by cervical dislocation at 30 min after injection. Whole brain, liver, lung, heart, kidney, spleen, adrenal, small intestine, pancreas, and blood samples were quickly removed and weighed. The radioactivity concentrations presenting in the various tissues were measured with the autogamma counter and expressed as percentages of the injected dose per gram of wet tissue (%ID/g). All radioactivity measurements were corrected for decay.

■ ASSOCIATED CONTENT

Supporting Information. HPLC separation charts of [^{11}C]**3a**−**c**. HPLC analysis charts of [^{11}C]**3a**−**c**. PET study with [^{11}C]**1** in normal rat: time−activity curves after injection of [^{11}C]**1**. PET study with [^{11}C]**3a**−**c**: maximum inhibitory percentages (%) of total uptake by pretreatment with **1** or **2** after injection of [^{11}C]**3a**−**c**. PET study with [^{11}C]**1** in lung inflammation (control vs inflammation): time−activity curves after injection of [^{11}C]**1**. This material is available free of charge via the Internet at http://pubs.acs.org.

■ AUTHOR INFORMATION

Corresponding Author

*Phone: 81-43-382-3708. Fax: 81-43-206-3261. E-mail: zhang@nirs.go.jp.

■ ACKNOWLEDGMENT

We are grateful to the staff of National Institute of Radiological Sciences for support with the cyclotron operation, radioisotope production, radiosynthesis, and animal experiments.

■ ABBREVIATIONS USED

AUC, area under time−activity curve; BOP, (benzotriazol-1-yloxy)tris(dimethylamino)phosphonium hexafluorophosphate; CH_2Cl_2, dichloromethane; [^{11}C]CO_2, [^{11}C]carbon dioxide; DMF, *N*,*N*-dimethyl formamide; DMSO, dimethyl sulfoxide; Et_3N, triethylamine; FAB-MS, fast atom bombardment mass spectra; FOV, field of view; HPLC, high-performance liquid chromatography; HRMS, high-resolution mass spectra; $LiAlH_4$, lithium aluminum hydride; LPS, lipopolysaccharide; MeCN, acetonitrile; MeI, methyl iodide; [^{11}C]MeI, [^{11}C]methyl iodide; $NaBH_4$, sodium borohydride; NaH, sodium hydride; PBR, peripheral-type benzodiazepine receptor; PBS, phosphate buffer solution; PET, positron emission tomography; SUV, standardized uptake value; TAC, time−activity curve; THF, tetrahydrofuran; t_R, retention time; TSPO, translocator protein (18 kDa)

■ REFERENCES

(1) Papadopoulos, V.; Baraldi, M.; Guilarte, T. R.; Knudsen, T. B.; Lacapère, J. J.; Lindemann, P.; Norenberg, M. D.; Nutt, D.; Weizman, A.; Zhang, M.-R.; Gavish, M. Translocator protein (18 kDa): new nomenclature for the peripheral-type benzodiazepine receptor based on its structure and molecular function. *Trends Pharmacol. Sci.* **2006**, *27*, 402–409.

(2) Braestrop, C.; Squires, R. F. Specific benzodiazepine receptors in rat brain characterized by high affinity [^{3}H]dizaepam binding. *Proc. Natl. Acad. Sci. U.S.A.* **1977**, *74*, 1839–1847.

(3) Gavish, M.; Bachman, I.; Shoukrun, R.; Katz, Y.; Veenman, L.; Weisinger, G. Enigma of the peripheral benzodiazepine receptor. *Pharmacol. Rev.* **1999**, *51*, 629–650.

(4) Chen, M. K.; Guilarte, T. R. Translocator protein 18 kDa (TSPO): molecular sensors of brain injury and repair. *Pharmacol. Ther.* **2008**, *118*, 57–65.

(5) Signore, A.; Mather, S. J.; Piaggio, G.; Malviya, G.; Dierckx, R. A. Molecular imaging of inflammation/infection: nuclear medicine and optical imaging agents and methods. *Chem. Rev.* **2010**, *110*, 3112–3145.

(6) Stoll, G.; Bendszus, M. Imaging of inflammation in the peripheral and central nervous system by magnetic resonance imaging. *Neuroscience* **2009**, *158*, 1151–1160.

(7) Winkeler, A.; Boisgard, R.; Martin, A.; Tavitian, B. Radioisotopic imaging of neuroinflammation. *J. Nucl. Med.* **2010**, *51*, 1–4.

(8) Maeda, J.; Zhang, M.-R.; Okauchi, T.; Ji, B.; Ono, M.; Hattori, S.; Kumata, K.; Iwata, N.; Saido, T. C.; Trojanowski, J. Q.; Lee, V. M.; Staufenbiel, M.; Tomiyama, T.; Mori, H.; Fukumura, T.; Suhara, T.; Higuchi, M. In vivo positron emission tomographic imaging of glial responses to amyloid-{beta} and tau pathologies in mouse models of Alzheimer's disease and related disorders. *J. Neurosci.* **2011**, *31*, 4720–4730.

(9) Scarf, A. M.; Kassiou, M. The translocator protein. *J. Nucl. Med.* **2011**, *52*, 1–4.

(10) Camsonne, R.; Crouzel, C.; Comar, D.; Maziere, M.; Prenant, C.; Sastre, J.; Moulin, M. A.; Syrota, A. Synthesis of *N*-[^{11}C]-methyl, *N*-(methyl-1-propyl), (chloro-2-phenyl)-1-isoquinoline carboxamide-3 (PK11195): a new ligand for peripheral benzodiazepine receptors. *J. Labelled Compd. Radiopharm.* **1984**, *21*, 985–991.

(11) Maeda, J.; Suhara, T.; Zhang, M.-R.; Okauchi, T.; Ichimiya, T.; Inaji, M.; Obayashi, S.; Suzuki, K. Novel peripheral benzodiazepine receptor ligand [^{11}C]DAA1106 for PET: an imaging tool for glial cells in the brain. *Synapse* **2004**, *51*, 283–291.

(12) Chauveau, F.; Boutin, H.; Van Camp, N.; Dollé, F.; Tavitian, B. Nuclear imaging of neuroinflammation: a comprehensive review of [^{11}C]PK11195 challengers. *Eur. J. Nucl. Med. Mol. Imaging* **2008**, *35*, 2304–2319.

(13) Dollé, F.; Luus, C.; Reynolds, A.; Kassiou, M. Radiolabelled molecules for imaging the translocator protein (18 kDa) using positron emission tomography. *Curr. Med. Chem.* **2009**, *16*, 2899–2923.

(14) Chauveau, F.; Boutin, H.; Van Camp, N.; Thominiaux, C.; Hantraye, P.; Rivron, L.; Marguet, F.; Castel, M. N.; Rooney, T.; Benavides, J.; Dollé, F.; Tavitian, B. In vivo imaging of neuroinflammation in the rodent brain with [^{11}C]SSR180575, a novel indoleacetamide radioligand of the translocator protein (18 kDa). *Eur. J. Nucl. Med. Mol. Imaging* **2011**, *38*, 509–514.

(15) Pike, V. W.; Taliani, S.; Lohith, T. G.; Owen, D. R.; Pugliesi, I.; Da Pozzo, E.; Hong, J.; Zoghbi, S. S.; Gunn, R. N.; Parker, C. A.; Rabiner, E. A.; Fujita, M.; Innis, R. B.; Martini, C.; Da Settimo, F. Evaluation of

novel N^1-methyl-2-phenylindol-3-ylglyoxylamides as a new chemotype of 18 kDa translocator protein-selective ligand suitable for the development of positron emission tomography radioligands. *J. Med. Chem.* **2011**, *54*, 366–373.

(16) Owen, D. R.; Gunn, R. N.; Rabiner, E. A.; Bennacef, I.; Fujita, M.; Kreisl, W. C.; Innis, R. B.; Pike, V. W.; Reynolds, R.; Matthews, P. M.; Parker, C. A. Mixed-affinity binding in humans with 18 kDa translocator protein ligands. *J. Nucl. Med.* **2011**, *52*, 24–32.

(17) Zhang, M.-R.; Kumata, K.; Maeda, J.; Yanamoto, K.; Hatori, A.; Okada, M.; Higuchi, M.; Obayashi, S.; Suhara, T.; Suzuki, K. ^{11}C-AC-5216: a novel PET ligand for peripheral benzodiazepine receptors in the primate brain. *J. Nucl. Med.* **2007**, *48*, 1853–1861.

(18) Miyoshi, M.; Ito, H.; Aragawa, R.; Takahashi, H.; Takano, H.; Higuchi, M.; Okumura, M.; Otsuka, T.; Kodaka, F.; Sekine, M.; Sasaki, T.; Fujie, A.; Seki, C.; Maeda, J.; Nakao, R.; Zhang, M.-R.; Fukumura, T.; Matsumoto, M.; Suhara, T. Quantitative analysis of peripheral benzodiazepine receptor in the human brain using PET with ^{11}C-AC-5216. *J. Nucl. Med.* **2009**, *50*, 1095–1101.

(19) Yui, J.; Maeda, J.; Kumata, K.; Kawamura, K.; Yanamoto, K.; Yamasaki, T.; Hatori, A.; Nengaki, N.; Higuchi, M.; Zhang, M.-R. ^{18}F-FEAC and ^{18}F-FEDAC: Monkey PET and imaging of translocator protein(18 kDa) in the brains of infarcted rats. *J. Nucl. Med.* **2010**, *51*, 1301–1309.

(20) Kita, A.; Kohayakawa, H.; Kinoshita, T.; Ochi, Y.; Nakamichi, K.; Kurumiya, S.; Furukawa, K.; Oka, M. Antianxiety and antidepressant-like effects of AC-5216, a novel mitochondrial benzodiazepine receptor ligand. *Br. J. Pharmacol.* **2004**, *142*, 1059–1072.

(21) Hardwick, M. J.; Chen, M. K.; Baidoo, K.; Pomper, M. G.; Guilarte, T. R. In vivo imaging of peripheral benzodiazepine receptors in mouse lungs: biomarker of inflammation. *Mol. Imaging* **2005**, *4*, 432–438.

(22) Wang, H.; Pullambhatla, M.; Guilarte, T. R.; Mease, R. C.; Pomper, M. G. Synthesis of [^{125}I]iodoDAP-713: a new probe for imaging inflammation. *Biochem. Biophys. Res. Commun.* **2009**, *389*, 80–83.

(23) Yanamoto, K.; Kumata, K.; Fujinaga, M.; Nengaki, N.; Takei, M.; Wakizaka, H.; Hosoi, R.; Momosaki, S.; Yamasaki, T.; Yui, J.; Kawamura, K.; Hatori, A.; Inoue, O.; Suzuki, K.; Zhang, M.-R. In vivo imaging and quantitative analysis of TSPO in rat peripheral tissues using small-animal PET with [^{18}F]FEDAC. *Nucl. Med. Biol.* **2009**, *37*, 853–860.

(24) Murata, A.; Masumoto, K.; Kondo, K.; Furukawa, K.; Oka, M. (Dainippon Sumitomo Pharma Co., Ltd.) 2-Aryl-8-oxodihydropurine derivatives. Japanese Patent JP 2001−48882A, 2011.

(25) Suzuki, K.; Inoue, O.; Hashimoto, K.; Yamasaki, T.; Kuchiki, M.; Tamate, K. Computer-controlled large scale production of high specific activity [^{11}C]Ro15−1788. *Appl. Radiat. Isot.* **1985**, *36*, 971–976.

(26) Zhang, M.-R.; Kida, T.; Noguchi, J.; Furutsuka, K.; Maeda, J.; Suhara, T.; Suzuki, K. [^{11}C]DAA1106: radiosynthesis and in vivo binding to peripheral benzodiazepine receptors in mouse brain. *Nucl. Med. Biol.* **2003**, *30*, 513–519.

(27) Fujinaga, M.; Yamasaki, T.; Kumata, K.; Kawamura, K.; Hatori, A.; Yanamoto, K.; Yui, J.; Yoshida, Y.; Ogawa, M.; Nengaki, N.; Maeda, J.; Fukumura, T.; Zhang, M.-R. Synthesis and evaluation of 6-[1-(2-[^{18}F]fluoro-3-pyridyl)-5-methyl-1*H*-1,2,3-triazol-4-yl]quinoline for positron emission tomography imaging of the metabotropic glutamate receptor type 1 in brain. *Bioorg. Med. Chem.* **2011**, *19*, 102–110.

(28) Pike, V. W. PET radiotracers: crossing the blood−brain barrier and surviving metabolism. *Trends Pharmacol. Sci.* **2009**, *30*, 431–440.

(29) Szaka, R. J.; Wang, N.; Gordon, L.; Nation, P. N.; Smith, R. H. A murine model of pulmonary damage induced by lipopolysaccharide via intranasal instillation. *J. Immunol. Methods* **1997**, *202*, 49–57.

(30) Harmsen, A. G. Role of alveolar macrophages in polysaccharide-induced neutrophil accumulation. *Infect. Immun.* **1988**, *56*, 1858–1863.

(31) Lefort, J.; Singer, M.; Leduc, D.; Renesto, P.; Nahori, M. A.; Huerre, M.; Creminon, C.; Chignard, M.; Vargaftig, B. B. Systemic administration of endotoxin induces bronchopulmonary hyperreactivity dissociated from TNF-alpha formation and neutrophil sequestration into the murine lungs. *J. Immunol.* **1998**, *161*, 474–580.

(32) Yanamoto, K.; Yamasaki, T.; Kumata, K.; Yui, J.; Odawara, C.; Kawamura, K.; Hatori, A.; Inoue, O.; Yamaguchi, M.; Suzuki, K.; Zhang, M.-R. Evaluation of *N*-benzyl-*N*-[^{11}C]methyl-2-(7-methyl-8-oxo-2-phenyl-7,8-dihydro-9*H*-purin-9-yl)acetamide ([^{11}C]DAC) as a novel translocator protein (18 kDa) radioligand in kainic acid-lesioned rat. *Synapse* **2009**, *63*, 961–971.

(33) Cheng, Y. C.; Prusoff, W. H. Relationship between inhibition constant (K_i) and the concentration of inhibitor which causes 50% inhibition (IC_{50}) of an enzymatic reaction. *Biochem. Pharmacol.* **1973**, *92*, 881–894.